Published online 24 March 2021

Nucleic Acids Research, 2021, Vol. 49, No. 9 ***4803–4815***
doi: 10.1093/nar/gkab162

NAR Breakthrough Article

microRNA-mediated translation repression through GYF-1 and IFE-4 in *C. elegans* development

Vinay K. Mayya[1,2], Mathieu N. Flamand[1,2], Alice M. Lambert[1,2], Seyed Mehdi Jafarnejad[3], James A. Wohlschlegel[4], Nahum Sonenberg[1,2] and Thomas F. Duchaine[1,2,*]

[1]Goodman Cancer Research Center, McGill University, Montréal H3G 1Y6, Canada, [2]Department of Biochemistry, McGill University, Montréal H3G 1Y6, Canada, [3]Patrick G. Johnston Centre for Cancer Research, Queen's University of Belfast, Belfast BT9 7AE UK and [4]Department of Biological Chemistry, David Geffen School of Medicine, University of California, Los Angeles, CA 90095, USA

Received January 11, 2021; Revised February 24, 2021; Editorial Decision February 25, 2021; Accepted March 17, 2021

ABSTRACT

microRNA (miRNA)-mediated gene silencing is enacted through the recruitment of effector proteins that direct translational repression or degradation of mRNA targets, but the relative importance of their activities for animal development remains unknown. Our concerted proteomic surveys identified the uncharacterized GYF-domain encoding protein GYF-1 and its direct interaction with IFE-4, the ortholog of the mammalian translation repressor 4EHP, as key miRNA effector proteins in *Caenorhabditis elegans*. Recruitment of GYF-1 protein to mRNA reporters *in vitro* or *in vivo* leads to potent translation repression without affecting the poly(A) tail or impinging on mRNA stability. Loss of *gyf-1* is synthetic lethal with hypomorphic alleles of embryonic *miR-35–42* and larval (L4) *let-7* miRNAs, which is phenocopied through engineered mutations in *gyf-1* that abolish interaction with IFE-4. GYF-1/4EHP function is cascade-specific, as loss of *gyf-1* had no noticeable impact on the functions of other miRNAs, including *lin-4* and *lsy-6*. Overall, our findings reveal the first direct effector of miRNA-mediated translational repression in *C. elegans* and its physiological importance for the function of several, but likely not all miRNAs.

INTRODUCTION

microRNAs (miRNAs) are ∼22nt long RNA molecules that direct the regulation of a wide variety of biological processes by impinging on gene expression (1). While embedded into Argonaute proteins (ALG-1/2 in *Caenorhabditis elegans*) as part of the miRNA-induced silencing complex (miRISC), miRNAs guide the recognition of complementary regions located in the 3′untranslated regions (UTR) of messenger RNAs (mRNAs). Following target recognition, the GW182 protein (AIN-1/2 in *C. elegans*), a core component of miRISC, recruits effector proteins such as the CCR4-NOT deadenylase complex to silence genes through translational repression and/or mRNA decay (2,3).

The relative contribution of mRNA translational repression and decay in the overall silencing of miRNA targets under physiological conditions remains largely unclear. Noticeable mechanistic differences have emerged in distinct systems and cell types. Different concentrations of miRNAs and effectors, and the density and distribution of miRNA-binding sites in mRNA 3′UTRs are possible explanations for such differences (4). Several studies have suggested that translation repression is the initial effect of silencing and precedes mRNA decay (5–8), whereas other reports have argued that mRNA decay could account for the bulk of miRNA-mediated silencing (9).

A well-characterized translation inhibition mechanism involves a 5′-cap-binding protein, 4EHP (eIF4E2), which interferes with the recognition of the 5′-cap by the translation initiation complex eIF4F (10). In *Drosophila,* RNA-binding proteins Bicoid and Brain Tumor (Brat) recruit 4EHP to repress the translation of *caudal* and *hunchback* mRNAs, respectively, ensuring proper embryonic development (11,12). 4EHP-mediated translational regulation of *HoxB4* mRNA is also essential for murine germ cell development (13). More recent studies in mammalian cells have shown that 4EHP represses the translation of a select group of mRNAs, directed through recruitment of the

*To whom correspondence should be addressed. Tel: +1 514 398 8649 Email: thomas.duchaine@mcgill.ca
Present address: Mathieu N. Flamand, Department of Biochemistry, Duke University School of Medicine, Durham, NC 27710, USA.

miRISC/CCR4-NOT/DDX6/4E-T complex by miRNAs (14,15). 4EHP can also form a translation repressor complex with the GIGYF2 protein, which is involved in the silencing of miRNA reporters (16). Furthermore, knockout of *4ehp* or *Gigyf2* in mice causes prenatal and early postnatal lethality, respectively (17,18). However, the physiological importance of the 4EHP-GIGYF2 interaction for the function of miRNAs or for animal development is unknown.

When combined with mass spectrometry, affinity purification from various tissues and cells has been successful in identifying functional miRISC cofactors (19–21). Here, we performed comparative proteomics in *C. elegans* embryos on known components of the miRNA pathway and identified a novel miRISC cofactor, GYF-1, and its direct binding partner IFE-4, an ortholog of 4EHP. *gyf-1* mutations exacerbated the defects of certain miRNAs but did not impact others. Through genome editing and the derived cell-free miRNA-mediated silencing systems, we show that interactions between GYF-1 and IFE-4 generated potent translational repression of target mRNAs without eliciting their deadenylation or reducing their stability. Our results identify the first direct translational repressor in miRNA-mediated silencing in *C. elegans* and reveal its physiological significance in a subset of the developmental cascades governed by miRNAs.

MATERIALS AND METHODS

Worm strains

N2 Bristol (WT), *let-7(n2853)*, *wIs51(scm-1::gfp)*, VT2700(*wIs51(scm-1::gfp);dcr-1(bp132)*), FD237(*wIs51(scm-1::gfp);dcr-1(bp132);gyf-1(qe27)*), *glp-1(e2142)*, *nDf50(miR-35–41)*, MH2636(*otIs114(plim-6::gfp,rol-6(d))*,*lsy-6(ot150)*), FD81(*gyf-1(qe27)*;*otIs114(plim-6::gfp,rol-6(d))*,*lsy-6(ot150)*), FD76(*gyf-1(qe27)*), FD119(*gyf-1(qe39)*), FD152(*gyf-1(qe56)*), FD198(*gyf-1(qe71)*), FD199(*gyf-1(qe72)*), FD165(*sel-1*::*5boxb;glp-1(e2142)*), FD193(*sel-1*::*5boxb;glp-1(e2142);gyf-1(qe56)*), FD261(*sel-1::5boxb;glp-1(e2142);gyf-1(qe71)*), FD262(*sel-1::5boxb;glp-1(e2142); gyf-1(qe72)*). All strains were maintained at 16°C.

CRISPR

The different alleles of *gyf-1* and *sel-1* were generated using a modified protocol (22). mRNP complex was assembled with rCas9 and *in vitro*-transcribed modified sgRNA(F+E) (23). Injection mixes contained 1.2 μg/μl Cas9, 300 mM KCl, 12.5 mM HEPES pH 7.4, 50 ng/μl dpy-10 sgRNA, 200 ng/μl gene-specific sgRNA, 13.75 ng/μl dpy-10 repair ssODN and 110 ng/μl ssODN gene-specific repair template (see Supplementary Table S4). Approximately 15 germlines of N2 gravid adults grown on *cku-80* RNAi plates were injected. Roller (heterozygotes for *dpy-10*) or dumpy animals were screened for edits by PCR.

Immunoprecipitation (IP) and Multidimensional Protein Identification (MuDPIT)

Embryonic pellets expressing either wild-type (N2) or FLAG-tagged GYF-1 (FD119) were homogenized in lysis buffer (50 mM Tris–HCl pH 8, 150 mM NaCl, 1 mM EDTA, 1% Triton X-100 with Complete EDTA-free protease inhibitors [Roche]) and cleared by 17 500 × g centrifugation. The lysates were treated with RNaseA, and FLAG-tagged GYF-1 was purified using anti-FLAG M2 Affinity Gel (Sigma-Aldrich A2220). For each IP, 5 mg of proteins were used at a concentration of 2 mg/ml in lysis buffer. IP was carried out at 4°C for 2 h with 50 μl of bead slurry per IP. Beads were washed four times in lysis buffer, and proteins were eluted with ammonium hydroxide solution. One tenth of the eluate was resolved by SDS-PAGE, and western blot analysis was performed using an anti-FLAG-M2 antibody. Non-transgenic N2 embryos were used as controls for the purifications. MuDPIT was performed as described in (24).

RNAi

RNAi was performed as described in (25). The genomic sequence of *gyf-1* was amplified using the primers listed in Supplementary Table S4. Using the PCR products as a template, RNA was *in vitro* transcribed using the T7 MegaScript kit (Ambion). The RNA was then purified using mini Quick Spin RNA columns (Roche). Larval stage-4 (L4) animals were injected with 100 ng/μl dsRNA, and bursting phenotype was monitored in the injected mother's progeny.

Antibody generation

The GYF-1 polyclonal antiserum was raised against the GYF domain region of GYF-1 by injecting rabbits with purified recombinants of the GYF domain. Likewise, IFE-4 polyclonal antiserum was raised against the full region of IFE-4. The primers used to clone the constructs for producing the recombinants are listed in Supplementary Table S4. Serum was used at a 1:1000 dilution in Odyssey blocking buffer (Li-Cor).

qRT-PCR

Total RNA was extracted from *C. elegans* embryos using QIAzol (Qiagen) and subsequently digested with DNase I. For cDNA synthesis, RNA was reverse transcribed using the Bio-Rad iScript Supermix for 5 min at 25°C, 30 min at 42°C, and 1 min at 95°C. The cDNA was diluted four-fold in water before using it for PCR (Bio-Rad iQ Supermix), with the following cycling parameters: initial denaturation at 95° for 2 min, denaturation for 15 s at 95°C, 59°C for 30 s and 72°C for 30 s, for 40 cycles. Reactions were followed by a melting curve analysis with the Eppendorf Realplex instrument and software. The RNA levels were normalized using the delta-delta Ct method with *act-1* mRNA as an internal control. The primers used are listed in Supplementary Table S4.

Preparation of embryonic extracts, *in vitro* transcription, translation assays, deadenylation assays, and mRNA target cloning were performed as described in (26,27). In brief, embryonic extracts were incubated with mRNA (1 nM) at 16°C for 0 to 4.5 h, as indicated. Luciferase activities were measured using the Dual-Luciferase Reporter assay

system (Promega). For deadenylation assays, 1 ng of ^{32}P-labeled RNA was incubated in embryonic extracts for 0 to 3 h. Half-deadenylation times were calculated by determining the intersect of the non-deadenylated and deadenylated RNA species over time using polynomial regression (order 2), using quantification of autoradiography with ImageJ.

Protein expression and purification

All recombinant proteins were expressed in either BL21-CodonPlus (DE3)-RIPL or ArcticExpress (DE3) competent cells (Agilent Technologies) grown in LB medium overnight at 13–16°C. For GST-recombinants, the cells were lysed using a sonicator (FisherScientific) in GST-lysis buffer (10 mM Tris–HCl, pH 8.0, 150 mM NaCl, 1 mM EDTA) supplemented with lysozyme (500 μg/ml), 1% Triton-X100 and protease inhibitor cocktail (Sigma).

For His-tagged recombinants (IFE-4, PATR-1), the cells were lysed in His-lysis buffer (20 mM sodium phosphate, 0.5 M NaCl, 20 mM Imidazole, 10% glycerol) supplemented with lysozyme, Triton-X100, and protease inhibitor cocktail. The protein was purified from cleared cell lysate using Ni-Sepharose 6 Fast Flow resin (GE Healthcare) in a Poly-Prep column (Bio-Rad). Following multiple washing steps with His-lysis buffer containing 60 mM imidazole, recombinants were eluted in His-lysis buffer containing 250 mM imidazole. Each fraction was analyzed by SDS-PAGE and Coomassie staining. Pure fractions were then concentrated using 50K centrifugal filter units (Amicon).

GST pull-down

Approximately 5 μg of GST or GST-fusion proteins were incubated in glutathione–sepharose beads (GE Healthcare) in the GST-lysis buffer at 4°C overnight. The bead-bound proteins were then incubated in GST-lysis buffer containing 5% BSA at 4°C for 2 h. Meanwhile, His-tagged recombinants (∼50 μg) were pre-cleared in glutathione–sepharose beads. The pre-cleared protein was then incubated with bead-bound proteins in phosphate-buffered saline containing 0.1% Tween20 (PBST). After 2 h of incubation, the beads were washed three times with PBST containing 500 mM KCl and eluted with a 2×-SDS loading buffer. The pull-downs were then analyzed by SDS-PAGE and subsequent Coomassie staining. For specific detection of His-tagged recombinants, anti-His (1:1000) (Abcam) was used. Bound primary antibodies were detected using Goat anti-Mouse IRDye (1:10 000) using an Odyssey imaging system (Li-Cor).

RESULTS

Concerted proteomics identifies GYF-1 association with miRISC and 4EHP

To identify new components of the miRNA-Induced Silencing Complex (miRISC), we compared the interactomes of a miRISC core component AIN-1 (GW182 ortholog), the miRISC cofactor NHL-2 (28), and the scaffolding subunit of the CCR4-NOT deadenylase complex, NTL-1 (CNOT1 ortholog; (20)) using immunoprecipitation (IP) coupled with Multi-Dimensional Protein Identification Technology (MuDPIT) (29,30). Each Co-IP dataset included at least three independent biological replicates (three for NHL-2 [unpublished], three for NTL-1 and six for AIN-1), and proteins detected in control samples were removed. Among the common interactors shared between all three baits were known components of the miRNA-induced silencing mechanism, mRNP granules (P-body, germ granule components; (20)), and several novel interactors of unknown function. Among the latter was the uncharacterized protein C18H9.3, detected in 11 out of a total of 12 independent datasets (Figure 1A and Supplementary Table S1). Comparative alignment of the C18H9.3 protein sequence across other eukaryote proteomes revealed homology for a domain found in the yeast SMY2 protein, named Glycine-Tyrosine-Phenylalanine (GYF) domain (Figure 1B and Supplementary Table S2). The SMY2-type GYF domain which recognizes the proline-rich motif PPGΦ (where P = proline, G = glycine, Φ = any hydrophobic amino acid) (31) was implicated in translational control through the function of *hs*GIGYF2 proteins (18). Because C18H9.3 is the first *C. elegans* protein identified to encode this domain, we chose to name it GYF-1. To further confirm the physical interactions between GYF-1 and the miRISC, we performed reciprocal IP and MuDPIT using GYF-1 as bait. GYF-1 protein was immunoprecipitated from *C. elegans* embryos expressing an endogenous 3xFLAG-tagged protein engineered via CRISPR/Cas9 (Figure 1C, upper panel). A total of 32 proteins were detected in all 3 independent biological replicates that were absent in all untagged (N2) samples, among which are miRISC components AIN-2, paralog of AIN-1, and the miRNA-dedicated argonaute, ALG-1 (ranked 5 and 12, respectively) (Figure 1C, bottom panel and Supplementary Table S3). The 4EHP ortholog IFE-4 was recovered with 45.56% peptide coverage on average, above all other detected interactions, suggesting a stable and likely direct interaction.

Mammalian GIGYF2 and *dm*GIGYF proteins interact with 4EHP through the canonical motif YXYX$_4$LΦ (where Y = tyrosine, X = any amino acid, L = leucine, and Φ = any hydrophobic amino acid) (18,32). A similar motif, FXYX$_4$LΦ, is present in the N-terminal region of GYF-1 (Figure 1D, upper panel). To test whether GYF-1 directly interacts with IFE-4, we generated GST-tagged constructs encoding fragments of GYF-1 and a construct wherein the conserved IFE-4 binding motif was mutated to alanines (FXYX$_4$LΦ to AXAX$_4$AA). A stable interaction of IFE-4 with the N-terminal region of GYF-1 was detected, and the mutation of the IFE-4 binding motif strongly impaired this interaction (Figure 1D, bottom panel). Residual binding, above the background level, with the IFE-4 binding mutant suggests the possible presence of a distinct, weaker IFE-4 binding site. In agreement with this, a lesser interaction between the C-terminal fragment of GYF-1 and IFE-4 could be detected in the pull-down assay. Interestingly, while cloning full-length *gyf-1* cDNA, we detected a splice variant (*gyf-1 Δife-4 binding motif*) of *gyf-1,* which did not encode the canonical IFE-4 binding motif (Figure 1E). A GST pull-down with this isoform confirmed the loss of robust interaction of IFE-4 with GYF-1 (ΔIFE-4 binding motif). Together, these results confirm that the conserved IFE-4

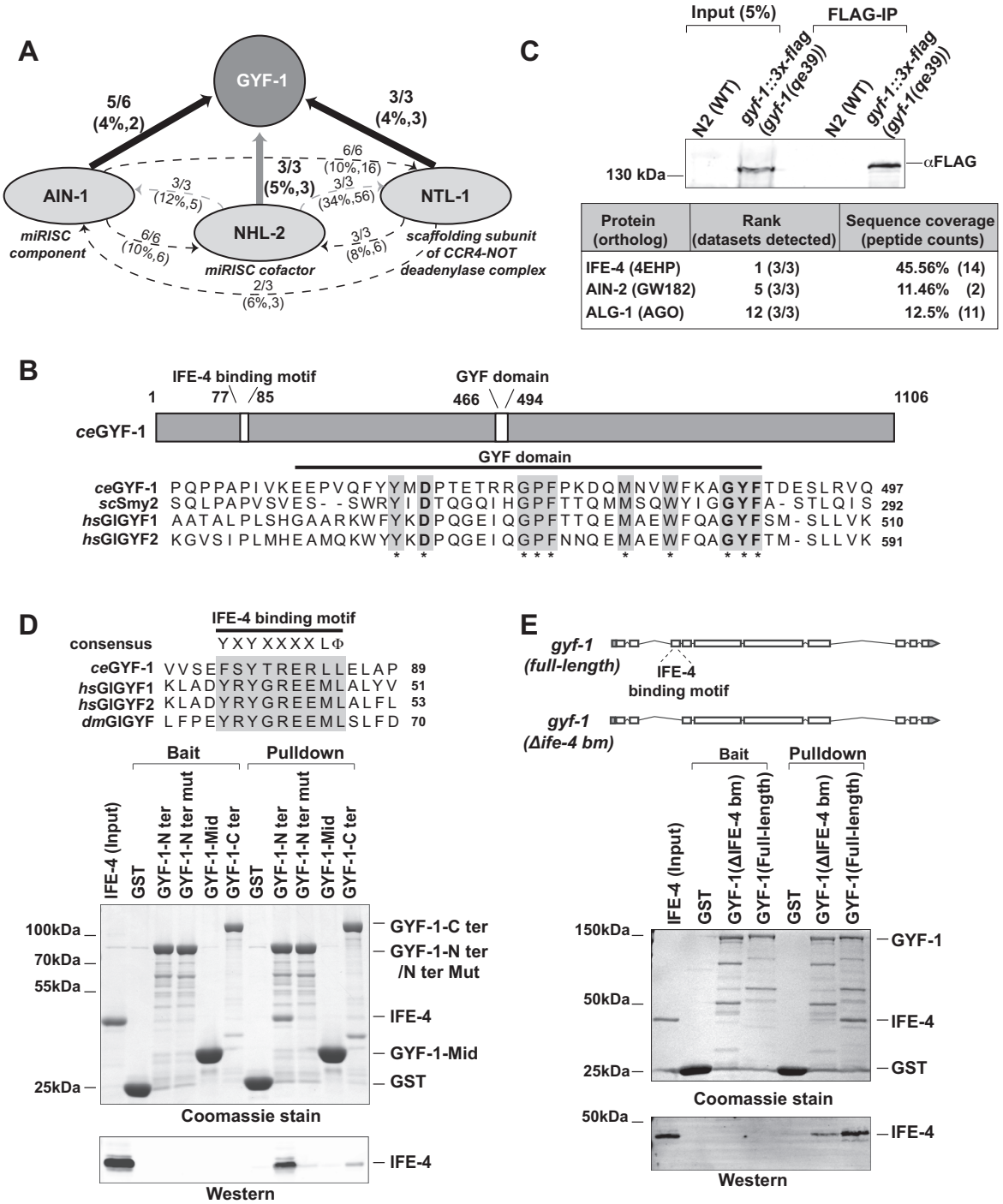

Figure 1. Concerted proteomics identifies GYF-1 association with miRISC and 4EHP. (**A**) A network of proteins converging on GYF-1, as detected by MuDPIT analyses in *C. elegans* embryonic extracts. FLAG immunoprecipitations were carried out on endogenously-tagged (genome-edited) AIN-1, NHL-2 and NTL-1. Arrowheads indicate detected interactions. The number of independent IPs in which GYF-1 was detected is indicated along with peptide coverage percentage and counts in brackets. Grey arrowheads indicate RNase A untreated interactions. (**B**) Schematic representation of the *ce*GYF-1 protein. The protein contains an N-terminal IFE-4 binding motif and a central GYF domain (top). The protein sequence of the C18H9.3 (*ce*GYF-1) GYF domain was aligned with other Smy2-type GYF domains (*Sc*Smy2, *hs*GIGYF1 and *hs*GIGYF2) (bottom). The conserved amino acids encompassing the GYF domain are highlighted in grey, while the amino acid Aspartate 466 that determines a Smy2-type GYF domain is in bold. (**C**) Western blot of embryo lysates and FLAG immunoprecipitations (FLAG-IP) from wild-type (N2) and animals expressing FLAG-tagged GYF-1 (top). The table indicates the proteins that were detected in GYF-1 MuDPIT analyses. The proteins were ranked based on NSAF values. (**D**) Sequence alignment of the IFE-4 binding motif present in *ce*GYF-1, *hs*GIGYF1/2, and *dm*GIGYF proteins. The consensus sequence $YXYX_4L\Phi$ is highlighted in grey (top). *In vitro* pull-down assay on GST-tagged WT or mutant fragments of GYF-1 and His-tagged IFE-4 purified recombinants (bottom). (**E**) Schematic representation of the two *gyf-1* isoforms: *gyf*-1 (full-length) and *gyf-1(Δife-4 binding motif)* (top). A GST pull-down assay showing the interaction between GST-tagged GYF-1 (full-length or ΔIFE-4 binding motif) with purified His-tagged IFE-4 (bottom). The input, baits, and pull-downs were analyzed by SDS-PAGE and Coomassie staining. Western blotting was performed using an anti-His antibody.

binding motif in the N-terminal region of GYF-1 is a direct binding site for IFE-4 and that this interaction may be subject to biological regulation by alternative splicing.

The GYF domain proteins can interact with several partners through the PPGΦ motif. A search for PPGΦ motif-containing proteins in factors with known function in post-transcriptional gene silencing (PTGS) identified the PPGL sequence in the mRNA decapping cofactor PATR-1 (ortholog of mammalian PatL1). To test whether GYF-1 can directly interact with PATR-1, we performed *in vitro* pull-down using full-length GST-tagged GYF-1 as bait and His-tagged PATR-1 as prey. GST-GYF-1 interacted with recombinant PATR-1, and mutation of the PATR-1 PPGL motif (to AAGA) abolished this interaction (Supplementary Figure S1A and B). Conversely, mutation of the GYF domain of GYF-1 abrogated the interaction with recombinant wild-type PATR-1 (Supplementary Figure S1C). This result shows that the GYF motif of GYF-1 interacts with the PPGL motif of PATR-1 *in vitro*, and possibly other proteins bearing this motif (see Discussion).

gyf-1 is synthetic lethal with *let-7* and *miR-35* hypomorphs

To investigate a possible role for GYF-1 in the miRNA-regulated developmental pathways, we engineered a loss-of-function (*lof*) allele by inserting a stop codon cassette in the fourth exon of *gyf-1* through CRISPR/Cas9 genome editing (*gyf-1(qe27)*) (Figure 2A). The lesion triggered mRNA destabilization, presumably through nonsense-mediated decay (NMD). Quantitative PCR analysis of *gyf-1* mRNA in embryos indicated a ∼5-fold reduction in mRNA (Supplementary Figure S2A). Western blot using a newly developed polyclonal antiserum confirmed that the bulk (>90%) of the GYF-1 protein signal was lost in this allele. A single band of unknown significance could still be seen, potentially reflecting another isoform (Supplementary Figure S2E). *gyf-1(qe27)* appeared WT at 16°C but was afflicted by a two-third reduction in brood size at 25°C (Supplementary Figure S2B). Notably, a pleiotropy of phenotypes could be observed at 25°C, including embryonic lethality, larval arrest, dumpy, high incidence of males, and low penetrance of the bursting vulva at the L4-to-adult transition (<5%) (Supplementary Figure S2C). Some of these phenotypes are compatible with defects in miRNA-induced silencing (33,34), but their complexity could indicate several other mechanisms of action and functions for GYF-1. To examine the role of *gyf-1* in miRNA-induced silencing, we employed a sensitized genetic assay based on the temperature-sensitive allele of *let-7(n2853)*. This allele encodes a point mutation in the seed sequence of *let-7* miRNA, which impairs the repression of the *lin-41* mRNA target and results in a temperature-sensitive vulval bursting at the L4-to-adult transition (34). The mild ∼20% penetrance of this phenotype at 16°C can be suppressed or exacerbated upon disruption of components of the miRISC or its cofactors (35). F1s from a cross between *gyf-1(qe27)* and *let-7(n2853)* animals were individually picked, and their progeny (F2) was monitored at the permissive temperature (16°C). In comparison with *let-7(n2853)* animals (26%), *let-7(n2853)*; *gyf-1(qe27/wt)* animals exhibited a striking increase in L4-to-adult bursting (61%) and 100% of the *gyf-1(qe27); let-7(n2853)* homozygous animals (20/20) died due to bursting, with no viable progeny recoverable (Figure 2B). Interestingly, the surviving *let-7(n2853)*; *gyf-1(qe27/wt)* heterozygous animals often died as young adults because of an egg-laying defect. This genetic interaction was further confirmed with point mutations in *gyf-1* (see below) and *gyf-1*(RNAi) by injection in *let-7(n2853)* animals (Supplementary Figure S2D). Together, these results show that *gyf-1 lof* is synthetic lethal with *let-7* and that this function is dosage-sensitive.

We next assayed for *gyf-1* genetic interactions with miRNAs implicated in other developmental events in *C. elegans*. The *miR-35–42* family of miRNAs is essential for early embryonic development (26,33). Its eight members are abundantly expressed in oocytes and early embryos (33,36,37), and animals expressing only *miR-42* (*nDf50*) are viable at lower temperatures (16°C) (33,38). To explore a possible role of GYF-1 in the functions of this family of miRNAs, *nDf50; gyf-1(qe27/wt)* were isolated and maintained at 16°C, and live progeny from individual picks was quantified (Figure 2C). Although *miR-35–41* deletion (nDf50) alone led to a reduced brood size (70 ± 21), the compound mutation strain *gyf-1(qe27)*; *nDf50* led to a near-complete eradication of any viable progeny (3 ± 3). However, this hypomorph was not as sensitive to *gyf-1* dosage as the *let-7(n2853)* mutant, as the brood size of the *nDf50; gyf-1(qe27/wt)* was virtually indistinguishable from *nDf50* animals. Together, these data demonstrate that loss of *gyf-1* greatly exacerbates *let-7* and *miR-35–41* deletion defects in embryogenesis and suggest that different miRNA cascades may exhibit different sensitivities to *gyf-1* dosage.

We further studied genetic interactions of *gyf-1* with other miRNA-involving developmental cascades. The *dcr-1(bp132)* mutant animals exhibit an increased number of seam cells and defects in alae formation that are visible in adult animals. This phenotype is thought to be attributed to the reduced levels of *lin-4* miRNA and misregulation of *lin-28* mRNA, but might also involve other miRNAs such as *miR-48*, *miR-84* and *miR-241* in early larval decisions (39,40). Notwithstanding this, the *gyf-1(qe27)* allele did not modify the phenotype of *dcr-1(bp132)* on seam cell numbers (Figure 2D). While wild-type and *dcr-1(bp132)* animals presented an average of 16 and 30 pairs of seam cells, respectively, when quantified with an *scm-1::gfp* reporter in young adults, loss of *gyf-1* did not significantly impact this phenotype. Lastly, *gyf-1* had no detectable impact on *lsy-6* function in left/right neuronal asymmetry (Figure 2E) in an ASEL/ASER reporter assay performed in the *lsy-6(ot150)* hypomorphic allele (41). Thus, our results show that while *gyf-1* is essential for the function of the miRNAs *let-7* and *miR-35–42* upon genetic perturbation, it does not appear to be required for the function of all miRNAs.

Loss of the IFE-4 binding motif or the GYF domain of GYF-1 exacerbate *let-7* defects

Next, we sought to corroborate the importance of the interaction between GYF-1 and IFE-4 for *let-7* activity by mutational analysis. For this, we mutated the sequence encoding the IFE-4 binding site in the *gyf-1* locus through CRISPR/Cas9 genome editing

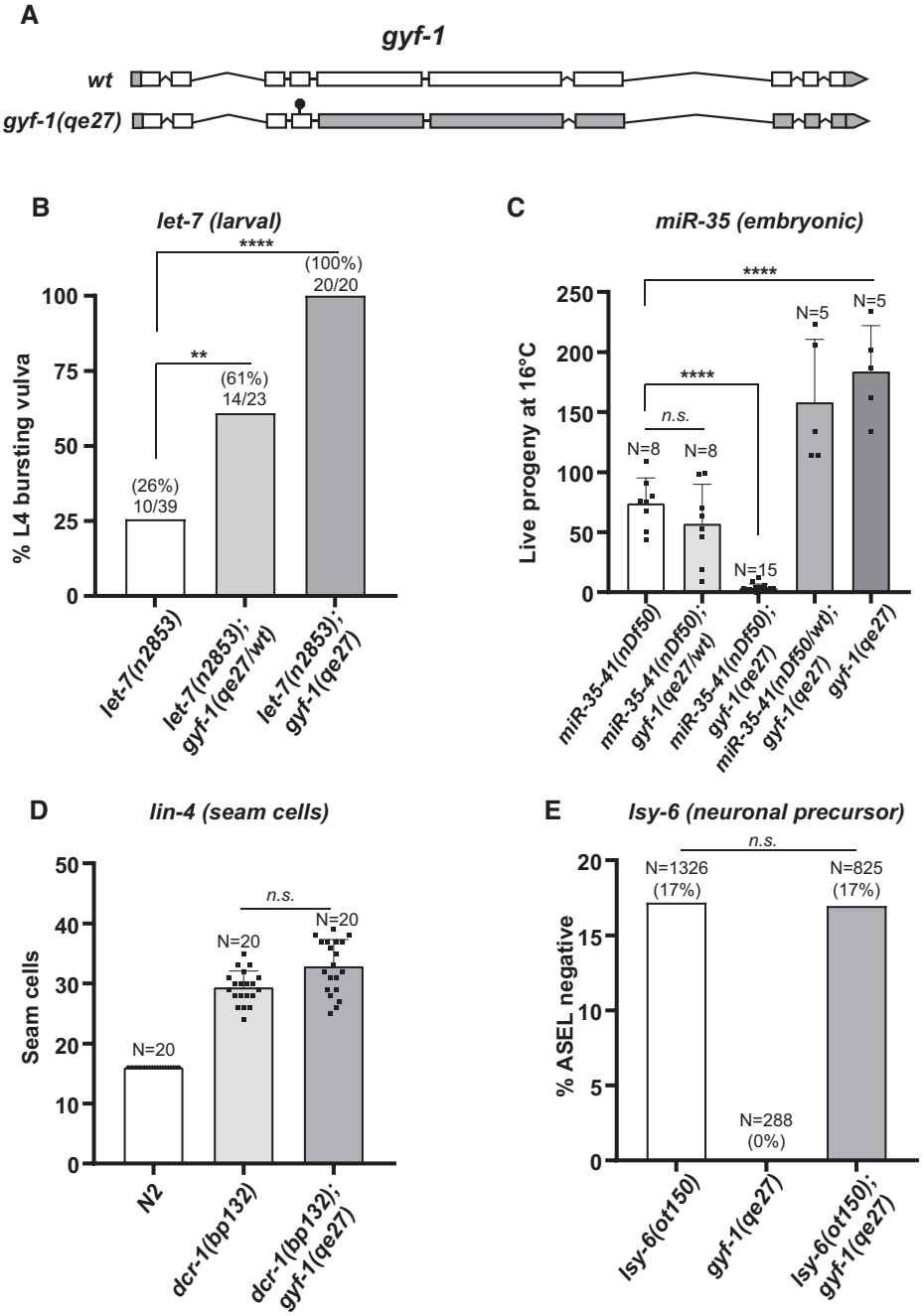

Figure 2. *gyf-1* is synthetic lethal with *let-7* and *miR-35* hypomorphs. (**A**) Schematic representation of the *gyf-1* locus, with the white and grey boxes indicating the coding and non-coding regions, respectively. A null allele of *gyf-1* was generated by inserting a stop codon (black circle) using the CRISPR/Cas9 gene-editing technique. (**B**) Percent bursting vulva phenotype was quantified at 16°C for animals with wild-type *gyf-1*, *gyf-1(qe27/wt)*, *gyf-1(qe27)* alleles in *let-7(n2853)* background. The number of bursting animals is indicated over the bars. Statistical significance was assessed using two-tailed chi-square analysis (****$P < 0.00005$, **$P < 0.005$). (**C**) Progeny produced by hermaphrodites of each genotype was counted at 16°C. Each black square within the bars indicates independent replicates. (**D**) Number of seam cells, quantified by the expression of seam cell-specific reporter *scm::gfp* in WT, *dcr-1(bp132)*, and *dcr-1(bp132);gyf-1(qe27)* animals. (**E**) Loss of ASEL-specific expression of *plim-6::gfp* reporter was quantified in *lsy-6* and *gyf-1* single mutants, and *lsy-6; gyf-1* double mutants. *N* = animals scored for each genotype. The error bars represent standard deviation and the *P*-value (****$P < 0.00005$) was determined using the two-tailed Student's *t*-test.

((FXYX$_4$LΦ to AXAX$_4$AA), *qe71*, referred henceforth as *gyf-1*$^{ife\text{-}4\ bm}$). This engineered genomic lesion effectively disrupted the interaction between GYF-1 and IFE-4 in the co-immunoprecipitation assay (Supplementary Figure S2E). Using a similar approach, we generated the *gyf-1(qe72)* mutant wherein conserved key residues involved in the GYF domain's interaction with PPGΦ-motif were mutated to alanines ((GYF to AAA), *gyf-1*$^{gyf\ dm}$) (Figure 3A). The two *gyf-1* mutant strains were then crossed with *let-7(n2853)*, and L4-to-adult bursting was quantified in the double mutants [*let-7(n2853); gyf-1*$^{ife\text{-}4\ bm}$ and *let-7(n2853); gyf-1*$^{gyf\ dm}$] (Figure 3B). Compared to the *let-7(n2853)* single mutant (24%), composite mutant strains with either *gyf-1*$^{ife\text{-}4\ bm}$ or *gyf-1*$^{gyf\ dm}$ exacerbated bursting to 56% and 39%, respectively. This result demonstrates that the IFE-4 binding motif, and to a lesser degree the GYF domain of GYF-1 partake in the *let-7* activity.

Genetic programs ensure developmental robustness to avert environmental stresses (42–45). For example, signaling cues from diapause signals correct cell lineage defects caused by shortages in *let-7* functions (46). We thus examined the impact of *gyf-1*$^{ife\text{-}4\ bm}$ and *gyf-1*$^{gyf\ dm}$ mutations on *let-7* functions in populations recovering from unfavorable (starvation) conditions. To this end, we induced L1 arrest by food deprivation (47) in *gyf-1*$^{ife\text{-}4\ bm}$*; let-7(n2853)* and *gyf-1*$^{gyf\ dm}$*; let-7(n2853)* animals and quantified L4-to-adult transition failure (bursting) in the recovering populations. Both mutations exacerbated the bursting phenotype observed in *let-7(n2853)* animals (26%), with 88% for *gyf-1*$^{ife\text{-}4\ bm}$*; let-7(n2853)* and 54% for the *gyf-1*$^{gyf\ dm}$*; let-7(n2853)* genotype (Figure 3C). Curiously, this exacerbation of the *let-7* phenotype by the *gyf-1*$^{ife\text{-}4\ bm}$ and *gyf-1*$^{gyf\ dm}$ mutations persisted in the next generation, indicating trans-generational inheritance (Supplementary Figure S3A). Lastly, to better delineate the contribution of the GYF-1 cofactor IFE-4 in *let-7* function, a null allele of *ife-4(ok320)* (48) was crossed with *let-7(n2853)* and *ife-4(ok320); let-7(n2853)*, and L4-to-adult bursting was quantified. 71% of the animals burst in comparison with 22% in the *let-7(n2853)* genotype (Figure 3D).

Overall, these results validate the functional importance of the GYF-1 and 4EHP proteins, and their direct interaction, in *let-7* functions and indicate that the GYF domain of GYF-1 also partakes in the *let-7* functions, although to a lesser extent. Furthermore, these results indicate that contribution of the IFE-4 binding motif and GYF domain can gain importance in developmental pathways upon environmental perturbations of nutrients or temperature.

GYF-1/4EHP is a potent translational repressor

To investigate the molecular function of GYF-1, we employed the λN:BoxB protein/mRNA tethering system (49,50) by engineering a strain wherein a sequence encoding the λN-tag was embedded in the *gyf-1* locus using CRISPR/Cas9 genome editing. Cell-free embryonic extracts, proficient for miRNA-mediated silencing and deadenylation (26,27), were then prepared from animals expressing either untagged (wt) or the GYF-1- λN fusion protein. *In vitro* transcribed *Renilla* luciferase (RL) reporters bearing 5BoxB sites or 3x-*miR-35* miRNA-binding sites (as a control) in their 3′ UTR region (Figure 4A) were incubated in the two extracts, along with a firefly luciferase (FL) internal control. mRNA and their expression were monitored using normalized luciferase assays (Figure 4B). Importantly, the control reporters were expressed in the two extracts with comparable efficiencies (Supplementary Figure S4A). In comparison to the control (wt) extract, RL reporters bearing 5BoxB sites were strongly repressed in the *gyf-1-λn* extract (Figure 4B). Tethering GYF-1 to the reporter mRNA led to more potent silencing (>95% repression) than the 3x-miR-35 reporter (∼70%) at the 3h time-point, which is known to be potently silenced through deadenylation (26). To determine if GYF-1 promotes mRNA deadenylation and/or destabilization *in vitro*, RL-5BoxB and RL-3xmiR-35 reporters were metabolically labeled with ^{32}P, and their stability was monitored after incubation in the different extracts through denaturing PAGE and autoradiography. The 3x-miR-35 reporter was rapidly deadenylated in both extracts, with a virtually indistinguishable deadenylation half-time ($t_{d1/2}$) (*wt*: 56 min versus *gyf-1-λn*: 52 min) (Figure 4C, Supplementary Figure S4B). Consistent with previous observations in *C. elegans* embryonic extracts (20,26), fully deadenylated mRNAs remained stable, and no acceleration of decay could be detected. No deadenylation or destabilization was detectable for the RL-5BoxB reporter in any of the tested extracts (Figure 4C). Taken together, these results show that GYF-1 recruitment to an mRNA directs potent translational repression without eliciting its deadenylation or destabilization.

We next tested the contribution of the IFE-4 binding motif and GYF domain of GYF-1 in translational repression by performing similar experiments in extracts derived from *gyf-1*$^{ife\text{-}4\ bm}$ and *gyf-1*$^{gyf\ dm}$ engineered strains (Figure 3) wherein the *gyf-1* locus also carried the λn-tag coding sequence. *N2 (wt)* extract where no λn fusion is tethered and *ain-2-λn* extracts where AIN-2 is tethered but does not lead to any silencing were used as negative controls. Tethering in the *gyf-1*$^{ife\text{-}4\ bm}$*-λn* extract entirely prevented the translational repression observed in the *wt gyf-1-λn* extract (Figure 4D). In contrast, silencing in the *gyf-1*$^{gyf\ dm}$*λn* extract did not significantly differ from the *wt gyf-1- λN*. Again, this was not due to batch-to-batch differences in the potency of extracts (Supplementary Figure S4A). Thus, these results show that GYF-1 requires IFE-4 protein to effect translational repression when recruited to an mRNA.

To confirm the molecular function of the GYF-1/IFE-4 effector complex-induced repression *in vivo*, we designed a genetic assay based on the activity of engineered GYF-1 mutants (wt, *gyf-1*$^{gyf\ dm}$, *gyf-1*$^{ife\text{-}4\ bm}$) on a CRISPR-edited endogenous mRNA reporter locus. The temperature-sensitive allele of *glp-1*(*e2142*) is embryonic lethal at non-permissive temperatures (21°C and above), and loss of *sel-1* expression suppresses this phenotype (51–53). Using CRISPR/Cas9 editing, 5BoxB sites were introduced in the 3′ UTR sequence of the *sel-1* locus (Figure 4E), and the engineered strain was crossed with strains expressing wt or mutant versions of GYF-1-λN fusion protein. Live progeny was then monitored at *glp-1*(*e2142*) non-permissive (21°C) temperature. As expected, animals expressing the *sel-1* mRNAs containing 5BoxB sites as part of their 3′ UTRs, but no GYF-1-λN fusion protein, did not produce viable progeny

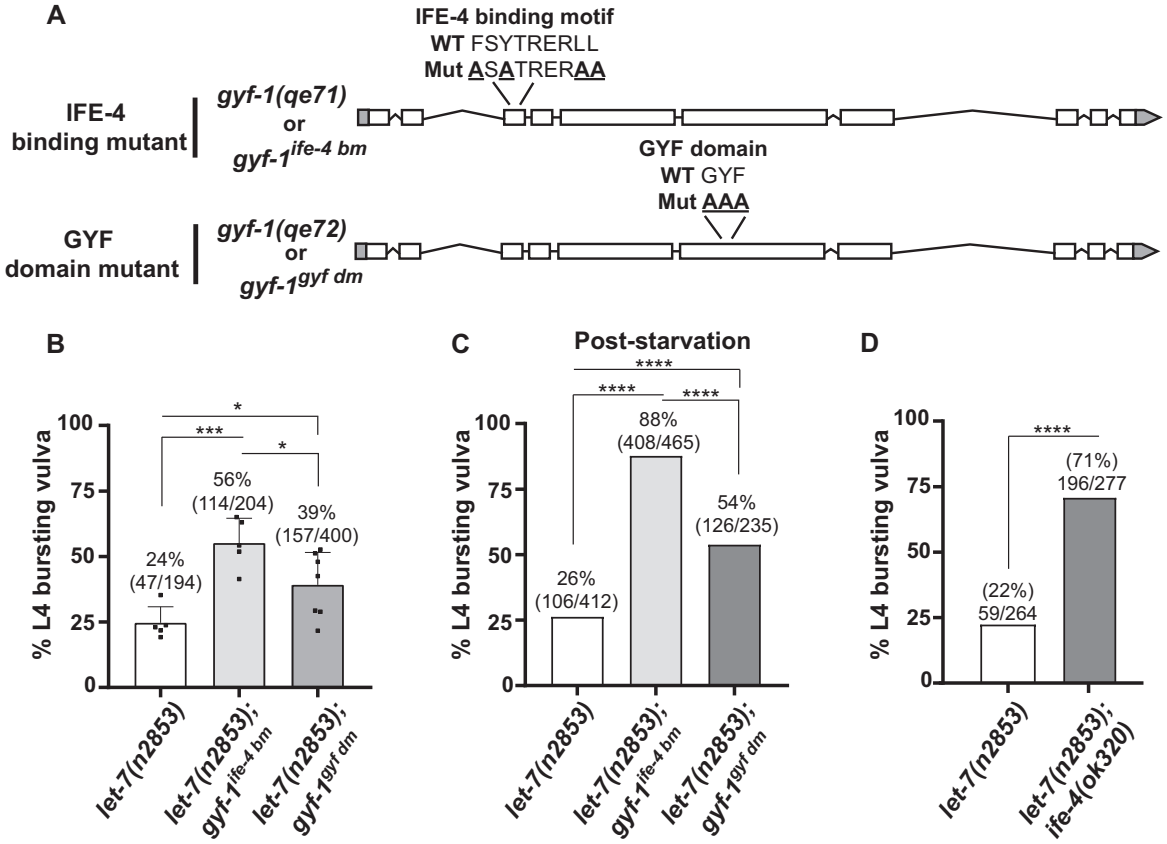

Figure 3. Loss of the IFE-4 binding motif or the GYF domain of GYF-1 exacerbate *let-7* defects. (**A**) A schematic representation of the two *gyf-1* mutants (*gyf-1*$^{ife\text{-}4\ bm}$and *gyf-1*$^{gyf\ dm}$) generated by the CRISPR/Cas9 gene-editing technique. The residues mutated are shown above the schematics. (**B**) Homozygous double mutants for both *let-7(n2853); gyf-1*$^{ife\text{-}4\ bm}$*/gyf-1*$^{gyf\ dm}$ were monitored for L4-to-adult bursting when maintained at 16°C. The number of bursting animals is indicated over the bars. The error bars represent standard deviation and the *P*-value (*** $P < 0.0005$, *$P < 0.05$) was determined using the two-tailed Student's *t*-test. (**C**) Animals grown in a food-deprived condition to induce stress were returned to favorable conditions, and percent L4 bursting vulva was monitored. (**D**) The percent bursting vulva phenotype was quantified at 16°C for animals with wild-type *ife-4* and *ife-4(ok320)* alleles in *let-7(n2853)* background. Statistical significance in (C) and (D) was assessed using two-tailed chi-square analysis (****$P < 0.0005$).

(Figure 4F, *no tethering*). Partial but effective rescue of embryonic lethality was observed in animals wherein wild-type GYF-1 was tethered to *sel-1* mRNA *in vivo*, indicating potent gene silencing (Figure 4F). qPCR analysis indicated no change in *sel-1* mRNA levels upon GYF-1 tethering (Supplementary Figure S4C), suggesting, as with *in vitro* experiments, translational repression without mRNA destabilization. Strikingly mirroring *in vitro* tethering results, *gyf-1*$^{ife\text{-}4\ bm}$ animals poorly suppressed *glp-1* phenotype, while *gyf-1*$^{gyf\ dm}$ suppressed embryonic lethality as well as *wt gyf-1-λn*.

Our results collectively indicate that GYF-1 is a potent translation repressor that primarily requires IFE-4 interaction to silence mRNAs both *in vitro* and *in vivo*, and that this silencing occurs without mRNA deadenylation or decay.

DISCUSSION

In this study, concerted interaction proteomics identified the GYF domain protein GYF-1 as a novel miRISC-associated protein in *C. elegans*. Precision genome engineering highlighted the physiological importance of GYF-1 interaction with the cap-binding IFE-4 protein in key developmental events orchestrated by the *miR-35* and *let-7* miRNAs. We further showed that GYF-1 directly interacts with IFE-4 to potently repress the translation of mRNAs without eliciting mRNA deadenylation and decay. Overall, our results support a model where GYF-1 acts as a cofactor of miRISC to repress the translation of a select subset of miRNA targets during the development of *C. elegans* (Figure 5).

Recent studies implicated the human and *Drosophila* homologs of GYF-1 in post-transcriptional gene silencing (16,32,54,55). In contrast to GYF-1, the homologs appear to function through translational repression and mRNA deadenylation and decay. *hs*GIGYF2, one of the two human GYF-1 homologs, silences miRNA reporters through interactions with 4EHP but also engages the CCR4-NOT deadenylase complex (56). *dm*GIGYF, the only known *Drosophila* homolog, interacts with 4EHP, Me31B (CGH-1/DDX6 ortholog), and HPat, the ortholog of PATR-1 (32,57), and silences luciferase reporters upon tethering in cell culture assays. Curiously, *dm*GIGYF has not been linked to miRNA-mediated silencing. The conservation of the mechanism by the GYF domain proteins will likely extend to a combination of translation repression, deadeny-

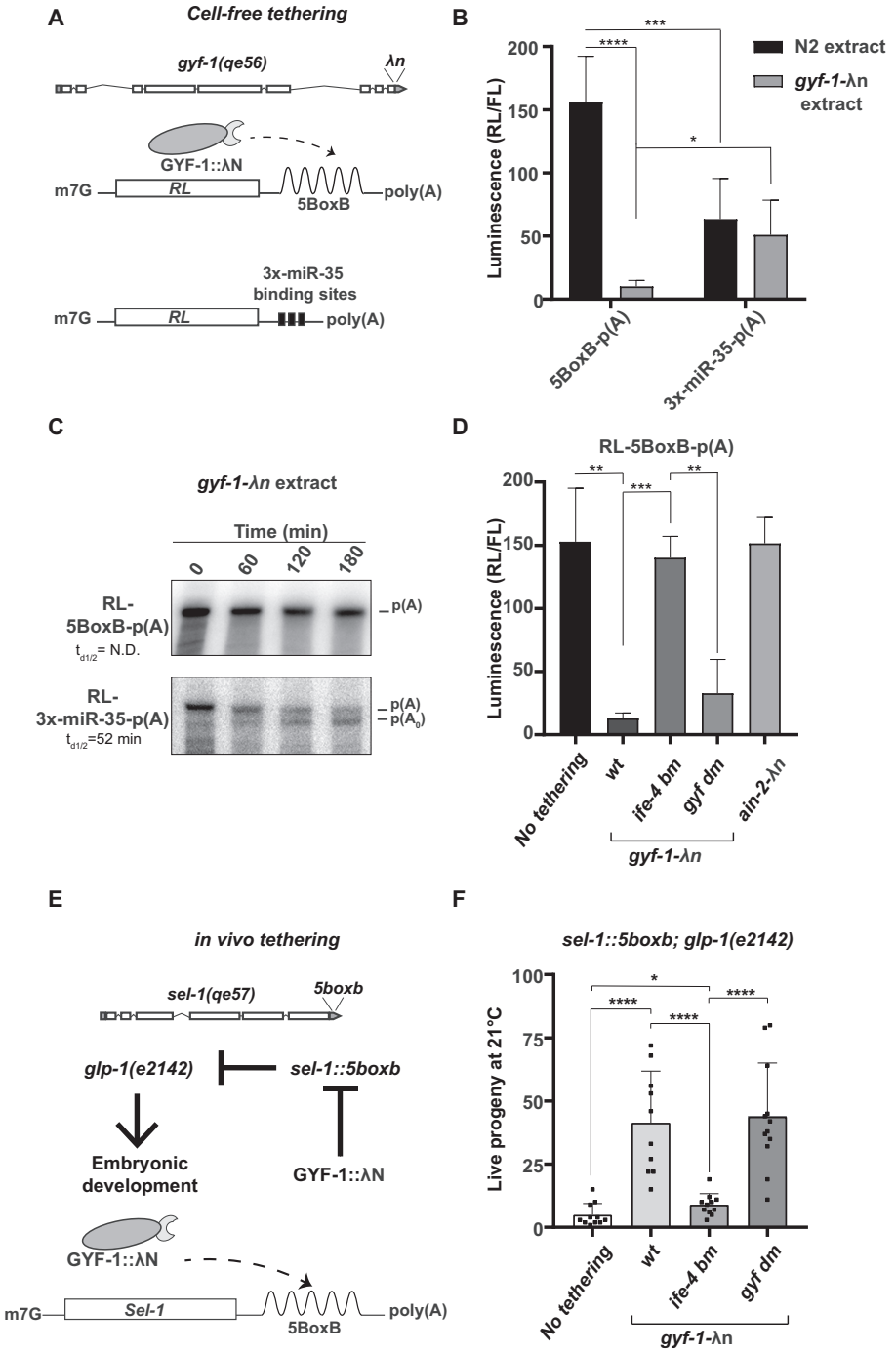

Figure 4. GYF-1/4EHP is a potent translational repressor. (**A**) A schematic representation of the *gyf-1* locus encoding a λN-tag at the C-terminus engineered through CRISPR/Cas9 (top). *In vitro* transcribed reporters were used to monitor translation and deadenylation activity in extracts derived from engineered strains (bottom). (**B**, **C**) Reporters bearing either 5boxB sites or 3× miR-35 binding sites were incubated in embryonic extracts expressing either wild-type (N2) or λN-tagged GYF-1. RL and FL activities were measured after 3 h using the dual-luciferase reporter assay system (Promega). RL activity was normalized to that of the FL control, $n = 6$ (B). The RNA was extracted at indicated time points and analyzed by UREA-PAGE (C). p(A) denotes the position of the adenylated reporter mRNA, while $p(A_0)$ indicates the position of the deadenylated reporter mRNA. Half-deadenylation rates ($t_{d1/2}$) were quantified using ImageJ. Images are representative of three independent experiments conducted using two different batches of extract preparations. $t_{d1/2}$ = N.D. indicates *not detected*. (**D**) Extracts expressing untagged-GYF-1 (no tethering), GYF-1-λN (WT), GYF-1-λN (IFE-4 BM/GYF DM), and AIN-2-λN were incubated with RL-5BoxB-p(A) reporters. RL and FL activities were measured as described in (B). RL activity was normalized to that of the FL control, $n = 3$. (**E**) The *sel-1* locus was engineered by the CRISPR/Cas9 gene-editing technique to encode 5BoxB sites in its 3′UTR (*sel-1(qe57)* (top). *Sel-1* loss-of-function can suppress the temperature-sensitive embryonic lethality phenotype in the loss-of-function mutation of *glp-1(e2142)* (middle). Animals expressing untagged-GYF-1 (No tethering) or λN-tagged GYF-1 (WT/IFE-4 BM/ GYF DM) were crossed with *sel-1(qe57); glp-1(e2142)* alleles. (bottom). (**F**) Live progeny of each genotype was counted at 21°C. Each black square within the bars indicates independent replicates, $n = 10$. The error bars represent standard deviation, and the *P*-value (**** $P < 0.00005$, *** $P < 0.0005$, ** $P < 0.005$, * $P < 0.05$) was determined using the two-tailed Student's *t*-test.

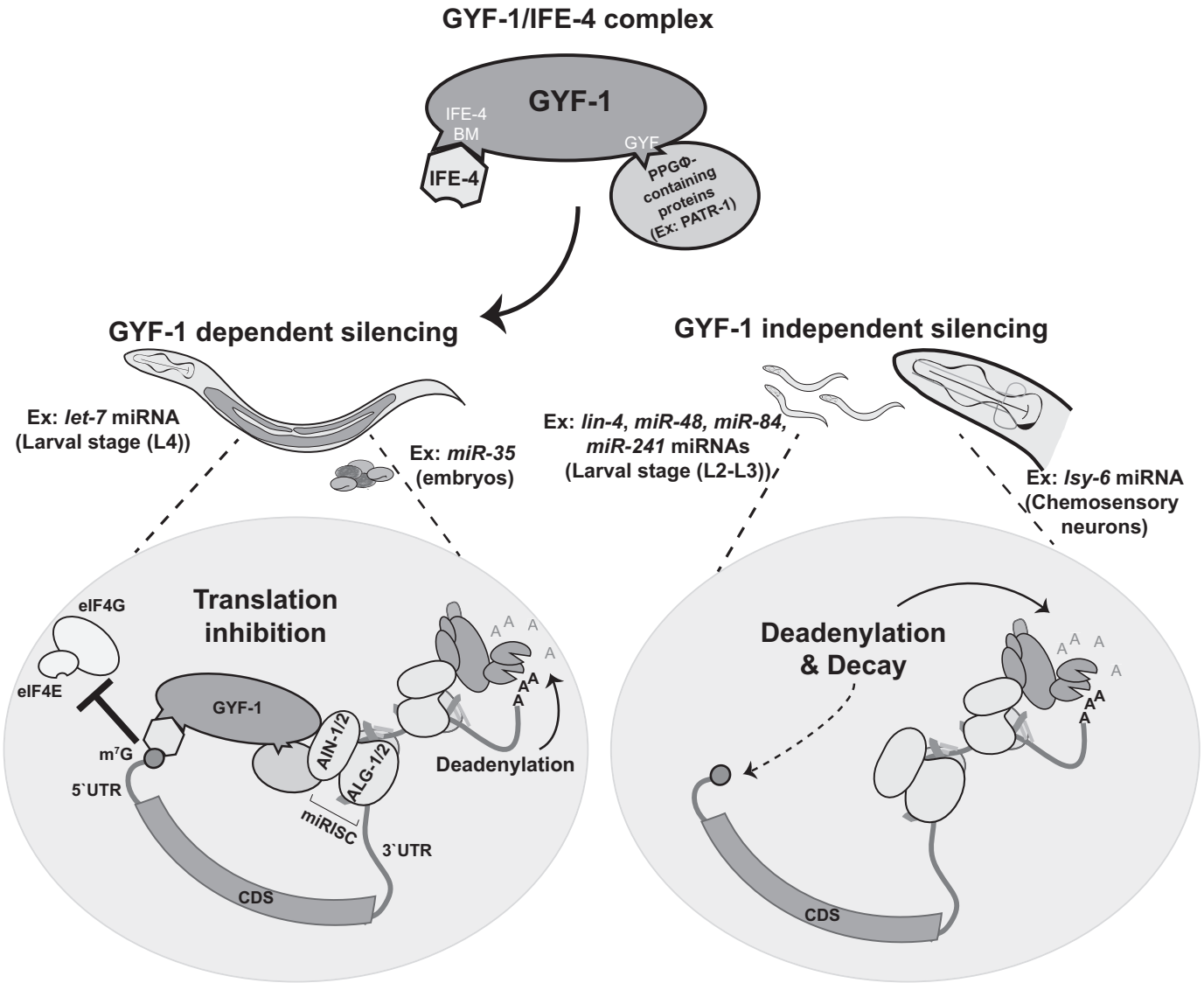

Figure 5. Model: GYF-1-dependency in miRNA-mediated silencing depends on developmental context. Through interactions with miRISC (larval *let-7* or embryonic *miR-35)*, the GYF-1/IFE-4 effector complex inhibits translation by interfering with the recognition of the 5′- cap by the translation initiation complex. For other miRNA/targets such as *lin-4, miR-48, miR-84, miR-241* (larval) and *lsy-6* (neuronal) miRNAs, GYF-1 is completely dispensable, and other silencing mechanisms such as deadenylation and decay fully compensate for the loss of GYF-1-mediated translation repression.

lation and decay. Beyond IFE-4/4EHP, the diversity of the effectors recruited by this family of protein will be reflected through the interactions of the GYF domain with binding partners bearing the PPGΦ motif. Here, we mapped a PATR-1 interaction with GYF-1 to the PPGΦ motif *in vitro* (Supplementary Figure S1). However, PATR-1 was not detected in our proteomic survey, and no evidence of decapping or decay, which could have been expected from such an interaction, was detected. While the orthologs of PATR-1 were characterized as de-capping cofactors, some studies indicate that they can also function as translation repressors (58,59). GYF-1 tethering to reporters elicited neither deadenylation nor decay, and mutation of the GYF domain had no impact on reporter silencing *in vitro*, in stark contrast with a mutation in the IFE-4/4EHP binding motif which fully impaired silencing. These results thus suggest that *C. elegans* GYF-1 primarily relies on its interaction with IFE-4 and translational repression to effect mRNA silencing. This view is in agreement with *in vivo* data as well, with results from the genetic interactions of the two modules of GYF-1 with the *let-7* hypomorph (Figure 3) and from *in vivo* tethering assays (Figure 4F). Notwithstanding this, the GYF domain did have a minor but significant contribution in target silencing in both assays, suggesting that PATR-1 and/or other PPGΦ motif-containing proteins participate in GYF-1/IFE-4-mediated translation repression. Additionally, the alternative splicing isoform GYF-1(ΔIFE-4 binding motif), which lacks the 4EHP-binding motif (Figure 1E), could reflect a physiological switch between silencing mechanisms. Fine mapping of the expression of this isoform may reveal the existence of other functions for the *gyf-1* gene, beyond its functions as a translational repressor. Alternatively, un-

der particular conditions of stoichiometry and interaction kinetics within the holo-miRISC, this isoform could act as a dominant-negative by competing with other effector proteins or complexes.

The subtle and mild phenotype of the *gyf-1* alleles on their own at 16°C drastically contrasts with their dosage-sensitive synthetic lethality with the *let-7* miRNA hypomorph. A plausible interpretation for this observation is that translational repression through GYF-1 is one of several effectors mobilized by miRISC, and that deadenylation and decay may partially but incompletely compensate for the loss of translational repression in the *gyf-1* mutant. Further attrition of silencing potency of one or several miRNA targets in hypomorphic alleles may thrust the gene regulation system beyond a phenocritical threshold. In addition, the distinct quality or kinetics of the different silencing effectors of miRISC could become critical during infection, disease, or environmental stress. The flexibility of the miRNA-mediated silencing mechanism and the importance of translation repression were also highlighted in embryonic stem cells wherein loss of DDX6, a cofactor of miRISC, leads to the translational upregulation of miRNA targets without eliciting mRNA decay (60). Our interpretation provides a refined perspective on a long-standing debate in the field of miRNA-mediated silencing: whether translational repression or mRNA decay accounts for the bulk of miRNA's silencing activities (2,5–9,61,62).

A similar interpretation may also explain the striking differences in the importance of GYF-1 for the function of *let-7* and *miR-35* miRNAs on the one hand, and the absence of detectable functional implication in the *lsy-6* and *lin-4* cascades on the other (Figures 2 and 5). Our data aligns with a growing number of publications based on model organisms, which indicate that miRISC effector activities change according to cellular and mRNA contexts (20). For example, as a result of extracellular cues, cells assemble functionally different miRISCs in *Drosophila* (63). Another recent study showed how differences in the composition of miRISC between germline and somatic tissues led to different mechanistic outcomes (64). Lastly, distinct 3′UTR sequences may mobilize different effectors as part of competitive or cooperative interactions, a theme that is prevalent in miRNA-mediated deadenylation in *C. elegans* embryo (26). Biochemical differences in miRISC composition or properties, their domain of expression, between the larval *let-7* and embryonic *lsy-6* cascades, for example, could thus explain the striking differences in GYF-1 impact in different developmental contexts.

Whether the involvement of GYF-1 is determined by cell fate or can differ between mRNAs and 3′UTR isoforms within the same expression domain remains to be investigated. The bursting phenotype at the L4-to-adult transition observed in *let-7*(*n2853*) alleles is accounted for by the misregulation of *lin-41* mRNA alone (34). In wild-type animals, *let-7* binds to the two complementary sequences in the 3′ UTR of *lin-41* and targets the mRNA for degradation (61), but homozygous *gyf-1 lof* leads to <5% bursting at the permissive temperature. This could be interpreted as *lin-41* mRNA decay being the prevalent mechanism in this cascade. Another interpretation is that this only reflects the contribution that cannot be compensated for, upon loss of miRNA-mediated translation repression through the GYF-1/IFE-4 complex. Revisiting the functional elements of the *lin-41* 3′ UTR in its native developmental context, and those of other phenocritical miRNA targets in different developmental cascades, is now more accessible than ever through precision genome editing. Careful re-examination of the mechanistic impact of those elements could provide a clearer view of the intersect, compensation or unique contribution of the effectors of miRNA-mediated silencing.

In conclusion, the discovery of the novel GYF-domain protein GYF-1 and precision genome-editing in *C. elegans* allowed a direct assessment of the physiological importance of miRNA-mediated translational repression in an animal's development and unveiled the surprising systems' flexibility among miRNA's silencing mechanisms.

DATA AVAILABILITY

Mass spectrometry proteomics data were deposited to the ProteomeXchange Consortium via the PRIDE partner repository, with the dataset identifier PXD023610.

Normalized spectral counts of proteins identified by MuDPIT in three independent GYF-1 purifications are listed in Supplementary Table S3.

SUPPLEMENTARY DATA

Supplementary Data are available at NAR Online.

ACKNOWLEDGEMENTS

We would like to apologize to authors whose directly related work may have not been cited in this manuscript. We thank Dr Victor Ambros for providing the *miR-35–41(nDf50)* strain and the Caenorhabditis Genetics Center (CGC) for the *glp-1(e2142)* and *ife-4(ok320)* strains used in this study.

FUNDING

Canadian Institutes of Health Research (CIHR) [MOP-123352 to T.F.D.]; The Charlotte and Leo Karassik Foundation PhD fellowship award (to V.K.M.). Funding for open access charge: Canadian Institutes of Health Research (CIHR) [MOP-123352].

Conflict of interest statement. None declared.

REFERENCES

1. Ameres,S.L. and Zamore,P.D. (2013) Diversifying microRNA sequence and function. *Nat. Rev. Mol. Cell Biol.*, **14**, 475.
2. Jonas,S. and Izaurralde,E. (2015) Towards a molecular understanding of microRNA-mediated gene silencing. *Nat. Rev. Genet.*, **16**, 421.
3. Duchaine,T.F. and Fabian,M.R. (2019) Mechanistic insights into MicroRNA-mediated gene silencing. *Cold Spring Harb. Perspect. Biol.*, **11**, a032771.
4. Iwakawa,H.-o. and Tomari,Y. (2015) The functions of MicroRNAs: mRNA decay and translational repression. *Trends Cell Biol.*, **25**, 651–665.
5. Djuranovic,S., Nahvi,A. and Green,R. (2012) miRNA-mediated gene silencing by translational repression followed by mRNA deadenylation and decay. *Science*, **336**, 237–240.
6. Bazzini,A.A., Lee,M.T. and Giraldez,A.J. (2012) Ribosome profiling shows that miR-430 reduces translation before causing mRNA decay in zebrafish. *Science*, **336**, 233–237.

7. Mathonnet,G., Fabian,M.R., Svitkin,Y.V., Parsyan,A., Huck,L., Murata,T., Biffo,S., Merrick,W.C., Darzynkiewicz,E., Pillai,R.S. *et al.* (2007) MicroRNA inhibition of translation initiation in vitro by targeting the cap-binding complex eIF4F. *Science*, **317**, 1764–1767.
8. Fabian,M.R., Mathonnet,G., Sundermeier,T., Mathys,H., Zipprich,J.T., Svitkin,Y.V., Rivas,F., Jinek,M., Wohlschlegel,J., Doudna,J.A. *et al.* (2009) Mammalian miRNA RISC recruits CAF1 and PABP to affect PABP-dependent deadenylation. *Mol. Cell*, **35**, 868–880.
9. Guo,H., Ingolia,N.T., Weissman,J.S. and Bartel,D.P. (2010) Mammalian microRNAs predominantly act to decrease target mRNA levels. *Nature*, **466**, 835–840.
10. Rom,E., Kim,H.C., Gingras,A.C., Marcotrigiano,J., Favre,D., Olsen,H., Burley,S.K. and Sonenberg,N. (1998) Cloning and characterization of 4EHP, a novel mammalian eIF4E-related cap-binding protein. *J. Biol. Chem.*, **273**, 13104–13109.
11. Cho,P.F., Poulin,F., Cho-Park,Y.A., Cho-Park,I.B., Chicoine,J.D., Lasko,P. and Sonenberg,N. (2005) A new paradigm for translational control: inhibition via 5′-3′ mRNA tethering by bicoid and the eIF4E cognate 4EHP. *Cell*, **121**, 411–423.
12. Cho,P.F., Gamberi,C., Cho-Park,Y.A., Cho-Park,I.B., Lasko,P. and Sonenberg,N. (2006) Cap-dependent translational inhibition establishes two opposing morphogen gradients in Drosophila embryos. *Curr. Biol.*, **16**, 2035–2041.
13. Villaescusa,J.C., Buratti,C., Penkov,D., Mathiasen,L., Planagumà,J., Ferretti,E. and Blasi,F. (2009) Cytoplasmic Prep1 Interacts with 4EHP Inhibiting Hoxb4 Translation. *PLoS One*, **4**, e5213.
14. Chapat,C., Jafarnejad,S.M., Matta-Camacho,E., Hesketh,G.G., Gelbart,I.A., Attig,J., Gkogkas,C.G., Alain,T., Stern-Ginossar,N., Fabian,M.R. *et al.* (2017) Cap-binding protein 4EHP effects translation silencing by microRNAs. *Proc. Natl. Acad. Sci. U.S.A.*, **114**, 5425–5430.
15. Jafarnejad,S.M., Chapat,C., Matta-Camacho,E., Gelbart,I.A., Hesketh,G.G., Arguello,M., Garzia,A., Kim,S.-H., Attig,J., Shapiro,M. *et al.* (2018) Translational control of ERK signaling through miRNA/4EHP-directed silencing. *eLife*, **7**, e35034.
16. Schopp,I.M., Amaya Ramirez,C.C., Debeljak,J., Kreibich,E., Skribbe,M., Wild,K. and Béthune,J. (2017) Split-BioID a conditional proteomics approach to monitor the composition of spatiotemporally defined protein complexes. *Nat. Commun.*, **8**, 15690.
17. Giovannone,B., Tsiaras,W.G., de la Monte,S., Klysik,J., Lautier,C., Karashchuk,G., Goldwurm,S. and Smith,R.J. (2009) GIGYF2 gene disruption in mice results in neurodegeneration and altered insulin-like growth factor signaling. *Hum. Mol. Genet.*, **18**, 4629–4639.
18. Morita,M., Ler,L.W., Fabian,M.R., Siddiqui,N., Mullin,M., Henderson,V.C., Alain,T., Fonseca,B.D., Karashchuk,G., Bennett,C.F. *et al.* (2012) A novel 4EHP-GIGYF2 translational repressor complex is essential for mammalian development. *Mol. Cell. Biol.*, **32**, 3585–3593.
19. Chu,C.-y and Rana,T.M. (2006) Translation repression in human cells by MicroRNA-Induced gene silencing requires RCK/p54. *PLoS Biol.*, **4**, e210.
20. Wu,E., Vashisht,A.A., Chapat,C., Flamand,M.N., Cohen,E., Sarov,M., Tabach,Y., Sonenberg,N., Wohlschlegel,J. and Duchaine,T.F. (2017) A continuum of mRNP complexes in embryonic microRNA-mediated silencing. *Nucleic Acids Res.*, **45**, 2081–2098.
21. Kakumani,P.K., Harvey,L.-M., Houle,F., Guitart,T., Gebauer,F. and Simard,M.J. (2020) CSDE1 controls gene expression through the miRNA-mediated decay machinery. *Life Sci Alliance*, **3**, e201900632.
22. Paix,A., Folkmann,A., Rasoloson,D. and Seydoux,G. (2015) High efficiency, homology-directed genome editing in caenorhabditis elegans using CRISPR-Cas9 ribonucleoprotein complexes. *Genetics*, **201**, 47–54.
23. Ward,J.D. (2015) Rapid and precise engineering of the Caenorhabditis elegans genome with lethal mutation co-conversion and inactivation of NHEJ repair. *Genetics*, **199**, 363–377.
24. Duchaine,T.F., Wohlschlegel,J.A., Kennedy,S., Bei,Y., Conte,D. Jr, Pang,K., Brownell,D.R., Harding,S., Mitani,S., Ruvkun,G. *et al.* (2006) Functional proteomics reveals the biochemical niche of C. elegans DCR-1 in multiple small-RNA-mediated pathways. *Cell*, **124**, 343–354.
25. Fire,A., Xu,S., Montgomery,M.K., Kostas,S.A., Driver,S.E. and Mello,C.C. (1998) Potent and specific genetic interference by double-stranded RNA in Caenorhabditis elegans. *Nature*, **391**, 806–811.
26. Wu,E., Thivierge,C., Flamand,M., Mathonnet,G., Vashisht,A.A., Wohlschlegel,J., Fabian,M.R., Sonenberg,N. and Duchaine,T.F. (2010) Pervasive and cooperative deadenylation of 3′UTRs by embryonic microRNA families. *Mol. Cell*, **40**, 558–570.
27. Wu,E. and Duchaine,T.F. (2011) Cell-free microRNA-mediated translation repression in Caenorhabditis elegans. *Methods Mol. Biol.*, **725**, 219–232.
28. Hammell,C.M., Lubin,I., Boag,P.R., Blackwell,T.K. and Ambros,V. (2009) nhl-2 Modulates microRNA activity in *Caenorhabditis elegans*. *Cell*, **136**, 926–938.
29. Wolters,D.A., Washburn,M.P. and Yates,J.R. (2001) An automated multidimensional protein identification technology for shotgun proteomics. *Anal. Chem.*, **73**, 5683–5690.
30. Washburn,M.P., Wolters,D. and Yates,J.R. 3rd (2001) Large-scale analysis of the yeast proteome by multidimensional protein identification technology. *Nat. Biotechnol.*, **19**, 242–247.
31. Kofler,M.M. and Freund,C. (2006) The GYF domain. *FEBS J.*, **273**, 245–256.
32. Ruscica,V., Bawankar,P., Peter,D., Helms,S., Igreja,C. and Izaurralde,E. (2019) Direct role for the Drosophila GIGYF protein in 4EHP-mediated mRNA repression. *Nucleic Acids Res.*, **47**, 7035–7048.
33. Alvarez-Saavedra,E. and Horvitz,H.R. (2010) Many families of C. elegans microRNAs are not essential for development or viability. *Curr. Biol.*, **20**, 367–373.
34. Ecsedi,M., Rausch,M. and Großhans,H. (2015) The let-7 microRNA directs vulval development through a single target. *Dev. Cell*, **32**, 335–344.
35. Flamand,M.N., Wu,E., Vashisht,A., Jannot,G., Keiper,B.D., Simard,M.J., Wohlschlegel,J. and Duchaine,T.F. (2016) Poly(A)-binding proteins are required for microRNA-mediated silencing and to promote target deadenylation in C. elegans. *Nucleic Acids Res.*, **44**, 5924–5935.
36. Lau,N.C., Lim,L.P., Weinstein,E.G. and Bartel,D.P. (2001) An abundant class of tiny RNAs with probable regulatory roles in *Caenorhabditis elegans*. *Science (New York, N.Y.)*, **294**, 858–862.
37. McJunkin,K. and Ambros,V. (2014) The embryonic mir-35 family of microRNAs promotes multiple aspects of fecundity in *Caenorhabditis elegans*. *G3 (Bethesda)*, **4**, 1747–1754.
38. Liu,M., Liu,P., Zhang,L., Cai,Q., Gao,G., Zhang,W., Zhu,Z., Liu,D. and Fan,Q. (2011) mir-35 is involved in intestine cell G1/S transition and germ cell proliferation in C. elegans. *Cell Res.*, **21**, 1605–1618.
39. Ren,H. and Zhang,H. (2010) Wnt signaling controls temporal identities of seam cells in *Caenorhabditis elegans*. *Dev. Biol.*, **345**, 144–155.
40. Ren,Z., Veksler-Lublinsky,I., Morrissey,D. and Ambros,V. (2016) Staufen negatively modulates MicroRNA activity in *Caenorhabditis elegans*. *G3 (Bethesda)*, **6**, 1227–1237.
41. Johnston,R.J. and Hobert,O. (2003) A microRNA controlling left/right neuronal asymmetry in *Caenorhabditis elegans*. *Nature*, **426**, 845–849.
42. Karp,X., Hammell,M., Ow,M.C. and Ambros,V. (2011) Effect of life history on microRNA expression during C. elegans development. *RNA*, **17**, 639–651.
43. Hammell,C.M., Karp,X. and Ambros,V. (2009) A feedback circuit involving let-7-family miRNAs and DAF-12 integrates environmental signals and developmental timing in *Caenorhabditis elegans*. *Proc. Natl. Acad. Sci. U.S.A.*, **106**, 18668.
44. Posadas,D.M. and Carthew,R.W. (2014) MicroRNAs and their roles in developmental canalization. *Curr. Opin. Genet. Dev.*, **27**, 1–6.
45. Li,X., Cassidy,J.J., Reinke,C.A., Fischboeck,S. and Carthew,R.W. (2009) A microRNA imparts robustness against environmental fluctuation during development. *Cell*, **137**, 273–282.
46. Ilbay,O. and Ambros,V. (2019) Pheromones and nutritional signals regulate the developmental reliance on let-7 family MicroRNAs in C. elegans. *Curr. Biol.*, **29**, 1735–1745.
47. Baugh,L.R. (2013) To grow or not to grow: nutritional control of development during *Caenorhabditis elegans* L1 arrest. *Genetics*, **194**, 539–555.
48. Dinkova,T.D., Keiper,B.D., Korneeva,N.L., Aamodt,E.J. and Rhoads,R.E. (2005) Translation of a small subset of *Caenorhabditis*

elegans mRNAs is dependent on a specific eukaryotic translation initiation factor 4E isoform. *Mol. Cell. Biol.*, **25**, 100–113.
49. Baron-Benhamou,J., Gehring,N.H., Kulozik,A.E. and Hentze,M.W. (2004) Using the lambdaN peptide to tether proteins to RNAs. *Methods Mol. Biol.*, **257**, 135–154.
50. Pillai,R.S., Artus,C.G. and Filipowicz,W. (2004) Tethering of human Ago proteins to mRNA mimics the miRNA-mediated repression of protein synthesis. *RNA*, **10**, 1518–1525.
51. Kodoyianni,V., Maine,E.M. and Kimble,J. (1992) Molecular basis of loss-of-function mutations in the glp-1 gene of *Caenorhabditis elegans*. *Mol. Biol. Cell*, **3**, 1199–1213.
52. Priess,J.R., Schnabel,H. and Schnabel,R. (1987) The glp-1 locus and cellular interactions in early C. elegans embryos. *Cell*, **51**, 601–611.
53. Flamand,M.N., Gan,H.H., Mayya,V.K., Gunsalus,K.C. and Duchaine,T.F. (2017) A non-canonical site reveals the cooperative mechanisms of microRNA-mediated silencing. *Nucleic Acids Res.*, **45**, 7212–7225.
54. Peter,D., Weber,R., Sandmeir,F., Wohlbold,L., Helms,S., Bawankar,P., Valkov,E., Igreja,C. and Izaurralde,E. (2017) GIGYF1/2 proteins use auxiliary sequences to selectively bind to 4EHP and repress target mRNA expression. *Genes Dev.*, **31**, 1147–1161.
55. Kryszke,M.H., Adjeriou,B., Liang,F., Chen,H. and Dautry,F. (2016) Post-transcriptional gene silencing activity of human GIGYF2. *Biochem. Biophys. Res. Commun.*, **475**, 289–294.
56. Amaya Ramirez,C.C., Hubbe,P., Mandel,N. and Bethune,J. (2018) 4EHP-independent repression of endogenous mRNAs by the RNA-binding protein GIGYF2. *Nucleic Acids Res.*, **46**, 5792–5808.
57. Peter,D., Ruscica,V., Bawankar,P., Weber,R., Helms,S., Valkov,E., Igreja,C. and Izaurralde,E. (2019) Molecular basis for GIGYF-Me31B complex assembly in 4EHP-mediated translational repression. *Genes Dev.*, **33**, 1355–1360.
58. Marnef,A., Maldonado,M., Bugaut,A., Balasubramanian,S., Kress,M., Weil,D. and Standart,N. (2010) Distinct functions of maternal and somatic Pat1 protein paralogs. *RNA*, **16**, 2094–2107.
59. Christou-Kent,M., Kherraf,Z.-E., Amiri-Yekta,A., Le Blévec,E., Karaouzène,T., Conne,B., Escoffier,J., Assou,S., Guttin,A., Lambert,E. *et al.* (2018) PATL2 is a key actor of oocyte maturation whose invalidation causes infertility in women and mice. *EMBO Mol. Med.*, **10**, e8515.
60. Freimer,J.W., Hu,T.J. and Blelloch,R. (2018) Decoupling the impact of microRNAs on translational repression versus RNA degradation in embryonic stem cells. *eLife*, **7**, e38014.
61. Bagga,S., Bracht,J., Hunter,S., Massirer,K., Holtz,J., Eachus,R. and Pasquinelli,A.E. (2005) Regulation by let-7 and lin-4 miRNAs results in target mRNA degradation. *Cell*, **122**, 553–563.
62. Eichhorn,S.W., Guo,H., McGeary,S.E., Rodriguez-Mias,R.A., Shin,C., Baek,D., Hsu,S.-H., Ghoshal,K., Villén,J. and Bartel,D.P. (2014) mRNA destabilization is the dominant effect of mammalian microRNAs by the time substantial repression ensues. *Mol. Cell*, **56**, 104–115.
63. Wu,P.-H., Isaji,M. and Carthew,R.W. (2013) Functionally diverse microRNA effector complexes are regulated by extracellular signaling. *Mol. Cell*, **52**, 113–123.
64. Dallaire,A., Frédérick,P.M. and Simard,M.J. (2018) Somatic and germline MicroRNAs form distinct silencing complexes to regulate their target mRNAs differently. *Dev. Cell*, **47**, 239–247.